Fluid–structure interaction within three-dimensional models of an idealized arterial wall

A. El Baroudi [a,*], F. Razafimahery [b], L. Rakotomanana [b]

[a] Arts et Métiers ParisTech, 2 bd du Ronceray, 49035 Angers, France
[b] IRMAR, Université de Rennes 1, Campus de Beaulieu, 35042 Rennes Cedex, France

A B S T R A C T

The ascending branch of the aorta is one of the most stressed organ of the arterial system. We aim to design a biomechanical model for analysing the aorta dynamics under a shock. The model includes the aorta layers and the influence of the blood pressure. We undertake a three-dimensional modal analysis of the coupled aorta–blood system. We determine in the present work the coupled natural frequencies and the modes shapes of the system of the aorta and blood. Three models are presented in this study: three-layers model, two-layers model and one layer model. For the analytical solving a potential technique is used to obtain a general solution for an aorta domain. The finite element model is then validated by these original analytical solutions. The results from the proposed method are in good agreement with numerical solutions.

Keywords:
Fluid–structure interaction
Modal analysis
Arterial wall
Finite element method
Multilayer

1. Introduction

Traumatic rupture of the thoracic aorta is commonly known as a fatal injury. The investigation and treatment of Blunt Traumatic Aortic Rupture (BTAR) or Blunt Traumatic Aortic Injury (BTAI) are nowadays well described. However, some uncertainty remains with regards of the pathogenic aetiology of BTAI. The injury and consequently the rupture are thought to be the result of both anatomic and mechanical factors. Initially, investigators proposed that BTAR was due to sudden increasing of arterial blood pressure. Later, recent theories suggest that injury or rupture result from a complex combination of mechanical stresses and is thus highly multi-parametric. Numerous factors are involved in the injury process but it remains uncertain to what extent, if any, each of them plays a part and under what circumstances. Of course, every mechanical force acting on the aorta may be important in the injury process (Zhao, Field, Diggers, & Richens, 2008). However, the relative importance of these forces still remains unclear and several different forces and hypotheses have been proposed over the years. It was thought that the injury was caused by a sudden stretching of the aorta. However, this mode of failure was probably not the only one since a cylindrical vessel under pressure would rupture axially rather than transversely. Then, some others attributed the occurrence of injury to a sudden increasing of blood pressure or also to the occurring of a water-hammer effect, which leads to high-pressure waves being reflected back along the vessel wall (Forman, Stacey, Evans, & Kent, 2008). Nevertheless, the water-hammer model is unable to consider the additional deformation of the aorta during an impact where increasing the curvature of the aorta could possibly lead to greater increases in the pressure wave in this region (Prosi, Perktold, Ding, & Friedman, 2004). More recent theories propose that aorta injury results from a

* Corresponding author.
E-mail address: adil.elbaroudi@ensam.eu (A. El Baroudi).

combination of mechanisms including shear, torsion and stretching (Zhao et al., 2008). These loadings are coupled with the blood pressure and propagation of wave within the aorta. To this end, it seems necessary to include the blood and the vessel undergoing deformation and interacting with the blood flow (Moore et al., 2008). In sum, there are still no definitive answers as to what the fundamental mechanisms are that cause this injury, though a great deal of speculation exists on what these might be. However, the high level of reproducibility of the site and nature of blunt traumatic rupture intuitively suggests that there is a reproducible mechanism of injury.

The largest artery in the body is the aorta. The highest fluid pressure in the body is the systolic pressure of the blood as it exits the heart into the large arterial system. The minimum pressure of this same blood is the diastolic pressure of the end of the heart's pumping cycle. The blood pressure in various parts of the body is also affected by accelerations of the body. The biomechanics within the ascending aorta characterizes the pressure and flow for the entire vascular system (see Fig. 1). One of the most stressed parts of the entire vascular system is the ascending branch of the aorta. Indeed, this branch is the first part of the system receiving the blood from the heart at the opening of the aortic valve, during the systolic phase. The study and the understanding of the dynamics of this branch is rather complicated due to the coupling effects and due to the heterogeneity of the organ radially.

The goal of this paper is to analyse the influence of the blood–aorta interaction on the coupled natural frequencies. Analytical method, based on the modal decomposition, and numerical method, based on the finite element method. We deal with modal analysis of the aorta with and without fluid (blood). For that purpose, analytical solutions of the coupled problem are obtained conversely to previous results (Zhang, 2002; Zhang, Liu, & Lam, 2001). Then the sensitivity of these natural frequencies and modal shapes is investigated with regards of the layers distribution. Wall properties are those used by Gao, Guo, Sakamoto, and Matsuzawa (2006). Solving the equation is based on the Helmholtz decomposition (Morse & Feshbach, 1946) of the wall displacement. This allows us to write the overall equation in terms of potentials. We assume an inertial coupling meaning that the longitudinal wave celerity is greater than any characteristic velocity of the blood flow. The blood is assumed compressible. One layer case, two layers case and three layers case are compared. Numerical solutions are compared with analytical results for assessing the reliability of the FEM software.

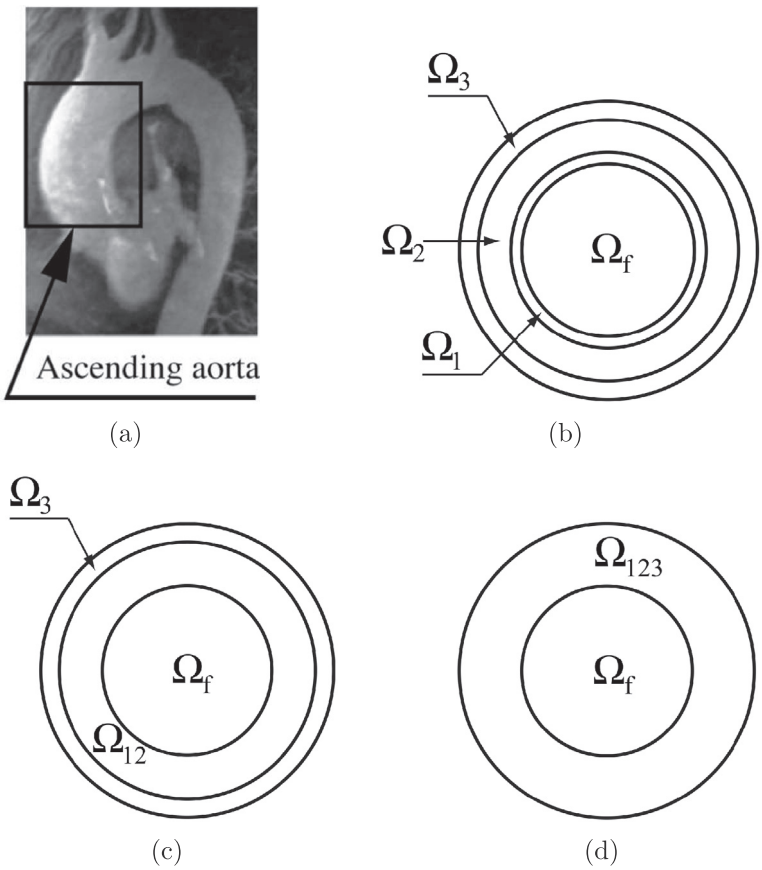

Fig. 1. Ascending aorta and its multi-layers cross sectional model: blood Ω_f, intima Ω_1, media Ω_2, adventitia Ω_3. (b) Three-layers model, (c) two-layers model and (d) one-layer model.

2. Frequency analysis of aorta

This paper tries to focuses in the study of the modal analysis of an idealized arterial wall. This step is needed before treating the dynamic response of the system. Modal analysis consists in linearizing the governing equations of nonlinear elasticity around an equilibrium position. In general the duration of a shock is very low and during the shock, the arterial wall undergoes a moderate deformation. In this case, the linear model seems to be more suitable. The domain occupied by the fluid is not confined, i.e. $R/th > 1$ (th and R are the thickness and the inner radius of the arterial wall, respectively), and $U_0/c_L \ll 1$ (U_0: characteristic velocity of the fluid; c_L: the compressional wave velocity in the solid), the fluid can be described by an inertial model where we can neglect the viscosity and the convective terms in the Navier–Stokes equations.

2.1. Structure of the arterial wall

The aorta is composed of three morphologically distinct layers: the intima, media, and adventitia, separated by internal and external elastic laminae. Adventitia is the outer layer of a blood vessel (Holzapfel, 2006). It is made up of connective tissue and is thicker in arteries than veins. This layer is known to give the arteries its longitudinal elasticity (e.g., Holzapfel, 2006). Media is the middle layer of a blood vessel. It is made up of smooth muscle tissue and some elastic fibers. It is much thicker in arteries than in veins. This layer is known to give the arteries its radial elasticity (e.g., Holzapfel & Gasser, 2007). Intima is the inner layer or lining of a blood vessel. It is made up of a single layer of endothelial cells with an underlining basement membrane, a connective tissue layer, and an elastic internal membrane.

Recent progress in biomedical imaging (e.g., Ou et al., 2005) allows us to extract very accurate data to reconstruct individualized 3D geometry of the artery and to obtain their kinematics and motion. Nevertheless, it is often necessary to analyse the sensitivity of the results with regards of the relative thickness of each layer and their relative stiffness. This is particularly true for investigating the dynamics of the aorta vs. the different layers. The goal of this work is to analyse the dynamic and wave motion of an aortic wall containing blood in flow by assuming acoustic situation for the blood. Three layers of the aorta are accounted for (e.g., Gao et al., 2006). We consider here the systolic phase where the motion is essentially radial. For most of examples treated in the present work, we use analytical method for solving the eigenvalue problems based on the Helmholtz decomposition since we consider domains with or without holes (e.g., Morse & Feshbach, 1946; Tsai, Young, Chen, & Fan, 2006). We solve the modal characteristics of the coupled system by assuming that stiffness of soft tissues surrounding the aorta does not influence the results. It means that the external wall is free of contact loadings. One-layer model, two-layers model and three-layers model are compared in this section.

2.2. Mathematical formulation

2.2.1. One-layer, two-layers and three-layers models of aorta

The three-layers model includes all layers although keeping in mind that biomedical imaging sometimes does not allow to distinguish them accurately. Geometry and regions are displayed on the figure (Fig. 2). Mechanical properties of the one-layer model and two-layers model are calculated from Gao et al. (2006). The arterial layers (Ω_i) are assumed to be made of an elastic solids where $i = 1, 2, 3$ indicates the intima ($i = 1$), media ($i = 2$) and the adventicia ($i = 3$), respectively. In fact for future studies, we plan to study the dynamic response of the arterial wall during a very short impact $\Delta t \ll 1$ s. This motivates

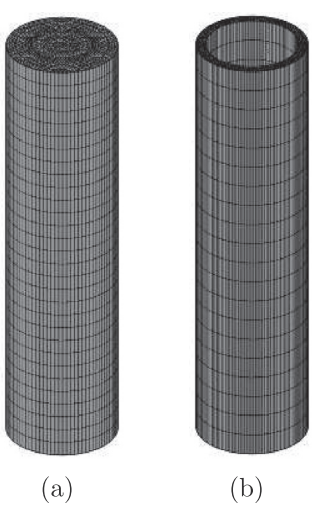

Fig. 2. The finite element mesh for arterial wall: (a) with and (b) without fluid.

the use of linear model. Indeed, for a very short impact, it is appropriate to use a linear behavior of the arterial wall. The vector of the displacement $\mathbf{u}^{(i)}$ of particles in an isotropic elastic material satisfies the Navier–Cauchy equations:

$$\rho_i \frac{\partial^2 \mathbf{u}^{(i)}(r,\theta,z,t)}{\partial t^2} = \mu_i \nabla^2 \mathbf{u}^{(i)}(r,\theta,z,t) + (\lambda_i + \mu_i)\nabla\nabla\cdot\mathbf{u}^{(i)}(r,\theta,z,t) \tag{1}$$

where ρ_i is the density, $\lambda_i,\ \mu_i$ are the Lamé constants, r is the radial direction, θ is the circumferential direction, z is the axial direction, t is time, and $\mathbf{u}^{(i)} = \left\{u_r^{(i)}, u_\theta^{(i)}, u_z^{(i)}\right\}^{\mathrm{T}}$ is the vector displacement along these directions.

The obtained equations of motion are highly complex and coupled. However, a simpler set of equations can be obtained by introducing scalar potentials $\phi_i,\ \psi_i$ and χ_i, known as the Helmholtz decomposition, such that

$$\mathbf{u}^{(i)} = \nabla\phi_i + \nabla\times(\psi_i\mathbf{e_z}) + \nabla\times\nabla\times(\chi_i\mathbf{e_z}) \tag{2}$$

Substituting Eq. (2) into Eq. (1) leads to three sets of partial differential equations

$$\nabla^2\phi_i = \frac{1}{c_{L_i}^2}\frac{\partial^2\phi_i}{\partial t^2}, \quad \nabla^2\psi_i = \frac{1}{c_{T_i}^2}\frac{\partial^2\psi_i}{\partial t^2}, \quad \nabla^2\chi_i = \frac{1}{c_{T_i}^2}\frac{\partial^2\chi_i}{\partial t^2} \tag{3}$$

where $\nabla^2 = \frac{\partial^2}{\partial r^2} + \frac{1}{r}\frac{\partial}{\partial r} + \frac{1}{r^2}\frac{\partial^2}{\partial\theta^2} + \frac{\partial^2}{\partial z^2}$, time dependence has the form $\exp(j\omega t)$ and $c_{L_i} = \sqrt{\frac{\lambda_i+2\mu_i}{\rho_i}}$ and $c_{T_i} = \sqrt{\frac{\mu_i}{\rho_i}}$ are the compressional and shear wave velocities in the solids, respectively. Applying the method of separation of variables, the solution of the equations for potentials, associated with an axial wave number k_z, radial wave number $(k_{\phi_i},\ k_{\psi_i})$ and circumferential mode parameter n, after considerable algebraic manipulations, can be shown to be

$$\phi_i = \left[A_i J_n(k_{\phi_i} r) + B_i Y_n(k_{\phi_i} r)\right]\cos(n\theta)\sin(k_z z)\exp(j\omega t) \tag{4}$$

$$\psi_i = \left[C_i J_n(k_{\psi_i} r) + D_i Y_n(k_{\psi_i} r)\right]\sin(n\theta)\sin(k_z z)\exp(j\omega t) \tag{5}$$

$$\chi_i = \left[E_i J_n(k_{\psi_i} r) + F_i Y_n(k_{\psi_i} r)\right]\cos(n\theta)\cos(k_z z)\exp(j\omega t) \tag{6}$$

$j = \sqrt{-1},\ k_z = m\pi/l,\ l$ is length of the tube, n and m are the azimuthal and axial wavenumbers. $n = 0, 1, 2, \ldots$, whereas k_z is found by satisfying the symmetry boundary condition on the $z = 0$ and $z = l$. Note that the displacement field $\mathbf{u}^{(i)}$ has components that are symmetric or antisymmetric in θ and z. Following standard practice, the solutions with symmetric (antisymmetric) axial velocities are called the antisymmetric (symmetric) axial modes, respectively, with k_z^a and k_z^s denoting the corresponding eigenvalues. Thus, we have $k_z^a = (m-1)\pi/l$ and $k_z^s = m\pi/l$ $(m = 0, 1, 2, \ldots)$. However, the azimuthal modes corresponding to $\cos(n\theta)$ and $\sin(n\theta)$ are really the same, due to periodicity in the azimuthal direction, i.e. there is no distinction in the values of n for the two families.

The radial wave number (k_{ϕ_i}, k_{ψ_i}) are related to the axial wave number k_z by $k_{\phi_i}^2 = \omega^2/c_{L_i}^2 - k_z^2,\ k_{\psi_i}^2 = \omega^2/c_{T_i}^2 - k_z^2$. ω denotes the angular frequency. J_n and Y_n are Bessel functions of the first and second kind of order n. $A_i,\ B_i,\ C_i,\ D_i,\ E_i$ and F_i are unknown coefficients which will be determined later by imposing the appropriate boundary conditions.

Using Eq. (2) the scalar components of the displacement vector $\mathbf{u}^{(i)}$ in cylindrical coordinates can be expressed by

$$u_r^{(i)} = \frac{\partial\phi_i}{\partial r} + \frac{n}{r}\psi_i - k_z\frac{\partial\chi_i}{\partial r} \tag{7}$$

$$u_\theta^{(i)} = \frac{nk_z}{r}\chi_i - \frac{n}{r}\phi_i - \frac{\partial\psi_i}{\partial r} \tag{8}$$

$$u_z^{(i)} = k_z\phi_i + k_{\psi_i}^2\chi_i \tag{9}$$

The stress tensor in the arterial layers $\sigma(\mathbf{u}^{(i)})$ is given by Hooke's law in terms of potentials as

$$\sigma_{rr}^{(i)} = 2\mu_i\left\{\frac{\partial^2\phi_i}{\partial r^2} - \frac{\lambda_i\omega^2}{2\mu_i c_{L_i}^2}\phi_i + \frac{n}{r^2}\left(r\frac{\partial\psi_i}{\partial r} - \psi_i\right) - k_z\frac{\partial^2\chi_i}{\partial r^2}\right\} \tag{10}$$

$$\sigma_{r\theta}^{(i)} = 2\mu_i\left\{\frac{n}{r^2}\left(\phi_i - r\frac{\partial\phi_i}{\partial r}\right) - \frac{\partial^2\psi_i}{\partial r^2} - \frac{k_{\psi_i}^2}{2}\psi_i + \frac{nk_z}{r^2}\left(r\frac{\partial\chi_i}{\partial r} - \chi_i\right)\right\} \tag{11}$$

$$\sigma_{rz}^{(i)} = \mu_i\left\{2k_z\frac{\partial\phi_i}{\partial r} + \frac{nk_z}{r}\psi_i + \left(k_{\psi_i}^2 - k_z^2\right)\frac{\partial\chi_i}{\partial r}\right\} \tag{12}$$

2.2.2. Fluid domain

In fluid–structure interaction problem, where the fluid medium is not confined (the volume occupied by the fluid is greater than the volume occupied by the solid), and when the ratio $U_0/c_L \ll 1$, the fluid can be described by a model without viscosity. This is the basic model in fluid–structure interaction model and is called inertial coupling (Axisa & Antunes, 2007). In this case the fluid (blood) is assumed non-viscous and isotropic which satisfies the acoustic wave equation. The equation of motion can be written as

$$\nabla^2 p - \frac{1}{c_f^2}\frac{\partial^2 p}{\partial t^2} = 0 \tag{13}$$

where p is the acoustic pressure and c_f is the speed of sound in a fluid medium. For a steady-state response in harmonic motion, the acoustic pressure becomes $p(r,\theta,z,t) = p(r,\theta,z)e^{-j\omega t}$. We substitute these expression in Eq. (13) we obtain the solution in cylindrical coordinates

$$p(r,\theta,z) = GJ_n(k_p r)\cos(n\theta)\sin(k_z z) \tag{14}$$

where $p(r,\theta,z)$ is the spatial acoustic pressure function, $k_p^2 = \omega^2/c_f^2 - k_z^2$ is the radial wave number and G is unknown constant to be determined by the boundary conditions. For incompressible fluid ($c_f \to \infty$), the basic governing equation is

$$\nabla^2 p = 0 \tag{15}$$

and the corresponding acoustic pressure can be obtained by simplifying Eq. (14)

$$p(r,\theta,z) = GI_n(k_z r)\cos(n\theta)\sin(k_z z) \tag{16}$$

where I_n is modified Bessel functions of the first kind of order n.

2.3. Fluid–structure interaction

First we define Γ ($r = R$), as the boundary contact between the fluid (blood) region and the intima region, Γ_1 ($r = R_1$), as the boundary contact between the intima region and the media region, Γ_2 ($r = R_2$), as the boundary contact between the media region and the adventitia region, and Γ_3 ($r = R_3$), as the outer boundary (the outer interface of the adventitia). The relevant boundary conditions that are physically realistic and mathematically consistent for this problem at the inner and outer surfaces of the elastic solid (arterial wall) in contact with fluid medium (blood) can be taken as follows:

- Continuity of fluid (blood) accelerations and the normal components of the intima accelerations:

$$\frac{\partial p(r,\theta,z)}{\partial r} = \rho_f \omega^2 u_r^{(1)}(r,\theta,z) \tag{17}$$

- Continuity of fluid (blood) pressures and the normal components of the intima stresses:

$$\sigma^{(1)} \cdot \mathbf{n} = -p\mathbf{n} \tag{18}$$

- Between the intima and the media, the displacements and normal stresses must be continuous, leading to:

$$\mathbf{u}^{(1)} = \mathbf{u}^{(2)} \tag{19}$$

$$\sigma^{(1)} \cdot \mathbf{n} = \sigma^{(2)} \cdot \mathbf{n} \tag{20}$$

- Between the media and the adventicia, the displacements and normal stresses must be continuous, leading to:

$$\mathbf{u}^{(2)} = \mathbf{u}^{(3)} \tag{21}$$

$$\sigma^{(2)} \cdot \mathbf{n} = \sigma^{(3)} \cdot \mathbf{n} \tag{22}$$

- The normal components of the adventicia stresses must be zero:

$$\sigma^{(3)} \cdot \mathbf{n} = \mathbf{0} \tag{23}$$

Combining these boundary conditions with Eqs. (7)–(12) and taking into account Eqs. (4)–(6), and (14) yield for each mode number (n,m) the following linear system

$$[\mathbf{M}]\{\mathbf{x}\} = \{\mathbf{0}\} \tag{24}$$

where

$$\{\mathbf{x}\} = \{G\ A_1\ B_1\ C_1\ D_1\ E_1\ F_1\ A_2\ B_2\ C_2\ D_2\ E_2\ F_2\ A_3\ B_3\ C_3\ D_3\ E_3\ F_3\}^T$$

$[\mathbf{M}]$ is a 19×19 matrix whose components are calculated using the Appendix A. For a non-trivial solution, the determinant of the matrix $[\mathbf{M}]$ must be equal to zero

$$\det[\mathbf{M}] = 0 \tag{25}$$

This equation indicates a relationship between the speed of sound in fluid and the elastic constants. The roots of Eq. (25) give the natural frequencies $f = \omega/2\pi$ of the cylindrical oscillations.

2.4. Numerical solution: weak formulation in ($\mathbf{u}^{(1)}$, $\mathbf{u}^{(2)}$, $\mathbf{u}^{(3)}$, p)

The used numerical formulations include the displacement formulation (Hamdi, Ousset, & Verchery, 1978), the potential formulation (Morand & Ohayon, 1979), the pressure formulation (Parthasarathi, Grosh, & Nuttall, 2000) and the combination

of some of them (Bathe, 1996). Finite element method is used to extract the natural frequencies and modal shapes. To compute the natural vibration modes of a fluid alone, the fluid is typically described either by pressure or by displacement potential variables. When the fluid is coupled with a solid, standard methods to solve Eqs. (1)–(6) consist in eliminating either the pressure or the displacement potential (Mellado & Rodrguez, 2001). However, in both cases non-symmetric eigenvalue problems are obtained (see, for instance, Zienkiewich & Taylor, 1989). To avoid this drawback, Morand and Ohayon introduce in Morand and Ohayon (1979) an alternative procedure which consists in using pressure and displacement potential simultaneously. In this section we summarize their approach; further details and discussions can be found in their book (Morand & Ohayon, 1995).

In order to obtain a weak formulation for Eqs. (1) and (13), firstly (1) is multiplied by a test function $\mathbf{v} = (\mathbf{v}_1, \mathbf{v}_2, \mathbf{v}_3) \in \mathbf{V}$ with

$$\mathbf{V} = \left\{ (\mathbf{v}_1, \mathbf{v}_2, \mathbf{v}_3) \in \mathbf{H}^1(\Omega_1) \times \mathbf{H}^1(\Omega_2) \times \mathbf{H}^1(\Omega_3),\ \mathbf{v}_3 = 0\ (\Gamma_3) \right\} \tag{26}$$

Now, by integrating by parts in Ω_1 (intima), Ω_2 (media) and Ω_3 (adventitia) (i.e., using Green's formula for tensor fields) and taking into account the boundary conditions, we obtain

$$\sum_{i=1}^{3} \left(\int_{\Omega_i} \sigma(\mathbf{u}^{(i)}) : \varepsilon(\mathbf{v}_i) dx - \omega^2 \int_{\Omega_i} \rho_i \mathbf{u}^{(i)} \cdot \mathbf{v}_i dx \right) - \int_{\Gamma} p\mathbf{n} \cdot \mathbf{v}_1 d\Gamma = 0 \tag{27}$$

Secondly, multiplying (13) by a test function $q \in Q = H^1(\Omega_f)$ and taking into account boundary conditions we get

$$\int_{\Omega_f} \nabla p \cdot \nabla q dx - \omega^2 \left(\int_{\Omega_f} \frac{pq}{c_f^2} dx + \int_{\Gamma} \rho_f \mathbf{u}^{(1)} \cdot \mathbf{n} q d\Gamma \right) = 0 \tag{28}$$

By using again Lagrange elements, where $\mathbf{u}_h^{(i)} \in \mathbf{P}_2 \times \mathbf{P}_2$ et $p_h \in \mathbf{P}_1$, discretization of the weak formulation induces a non symmetrical system

$$\begin{bmatrix} \mathbf{K}_1 & \mathbf{O} & \mathbf{O} & -\mathbf{B} \\ \mathbf{O} & \mathbf{K}_2 & \mathbf{O} & \mathbf{O} \\ \mathbf{O} & \mathbf{O} & \mathbf{K}_3 & \mathbf{O} \\ \mathbf{O} & \mathbf{O} & \mathbf{O} & \mathbf{K}_p \end{bmatrix} \begin{bmatrix} \mathbf{U}_1 \\ \mathbf{U}_2 \\ \mathbf{U}_3 \\ \mathbf{P} \end{bmatrix} = \omega^2 \begin{bmatrix} \mathbf{M}_1 & \mathbf{O} & \mathbf{O} & \mathbf{O} \\ \mathbf{O} & \mathbf{M}_2 & \mathbf{O} & \mathbf{O} \\ \mathbf{O} & \mathbf{O} & \mathbf{M}_3 & \mathbf{O} \\ \mathbf{M}^a & \mathbf{O} & \mathbf{O} & \mathbf{M}_p \end{bmatrix} \begin{bmatrix} \mathbf{U}_1 \\ \mathbf{U}_2 \\ \mathbf{U}_3 \\ \mathbf{P} \end{bmatrix} \tag{29}$$

where $\mathbf{U}_1$, $\mathbf{U}_2$, $\mathbf{U}_3$ and $\mathbf{P}$ are the vectors of nodal values for $\mathbf{u}^{(1)}$, $\mathbf{u}^{(2)}$, $\mathbf{u}^{(3)}$ and p, respectively, and the submatrices of Eq. (29) are defined by

$$\int_{\Omega_i} \sigma(\mathbf{u}^{(i)}) : \varepsilon(\mathbf{v}_i) dx = \mathbf{V}_i^T \mathbf{K}_i \mathbf{U}_i; \quad \int_{\Omega_i} \rho_i \mathbf{u}^{(i)} \cdot \mathbf{v}_i dx = \mathbf{V}_i^T \mathbf{M}_i \mathbf{U}_i$$
$$\int_{\Gamma} p\mathbf{v}_1 \cdot \mathbf{n} d\Gamma = \mathbf{V}_1^T \mathbf{B} \mathbf{P}; \quad \int_{\Gamma} \rho_f \mathbf{u}^{(1)} \cdot \mathbf{n} q d\Gamma = \mathbf{Q}^T \mathbf{M}^a \mathbf{U}_1$$
$$\int_{\Omega_f} \nabla p \cdot \nabla q dx = \mathbf{Q}^T \mathbf{M}_p \mathbf{P}; \quad \int_{\Omega_f} \frac{pq}{c_0^2} dx = \mathbf{Q}^T \mathbf{K}_p \mathbf{P}$$

for $i = 1, 2, 3$; where $\mathbf{V}_1$, $\mathbf{V}_2$, $\mathbf{V}_3$ and $\mathbf{Q}$ are the vectors of nodal values for $\mathbf{v}_1$, $\mathbf{v}_2$, $\mathbf{v}_3$ and q, respectively. $\mathbf{M}^a$ is the added mass matrix (symmetric and positive definite Morand & Ohayon, 1995). $\mathbf{K}_i$ (resp. $\mathbf{M}_i$) and $\mathbf{K}_p$ (resp. $\mathbf{M}_p$) are stiffness (resp. mass) matrices attributed to the aorta layer i and the blood respectively. The non symmetrical system (29) is solved by using Comsol Multiphysics software where a condensation technique is applied for avoiding spurious modes generally inherent to this class of problems.

3. Longitudinal, torsional, flexural and breathing mode vibration

The results presented in Eq. (25) are a general natural frequencies equation. For some simpler modes, the above mentioned method can be simplified. For example see the following.

3.1. Torsional mode vibration

The torsion mode vibration is such a mode in which the scalar components of the displacement $u_r^{(i)}$ and $u_z^{(i)}$ are zeros and only the circumferential displacement $u_\theta^{(i)}$ is independent of θ. This condition is achieved if $\phi_i = \chi_i = 0$. Through (8) and (11) this gives for the non-vanishing components of displacement and stresses

$$u_\theta^{(i)} = -\frac{\partial \psi_i}{\partial r}, \quad \sigma_{r\theta}^{(i)} = -2\mu_i \left\{ \frac{\partial^2 \psi_i}{\partial r^2} + \frac{k_{\psi_i}^2}{2} \psi_i \right\} \tag{30}$$

Thus, the general solution for ψ_i must be constructed from the set

$$\psi_i = \left[C_i J_0(k_{\psi_i} r) + D_i Y_0(k_{\psi_i} r)\right] \sin(k_z z) \exp(j\omega t) \tag{31}$$

In this case the boundary conditions Eqs. (17)–(23) become

$$\sigma_{r\theta}^{(1)}(r,z) = 0$$
$$u_\theta^{(1)}(r,z) = u_\theta^{(2)}(r,z), \quad \sigma_{r\theta}^{(1)}(r,z) = \sigma_{r\theta}^{(2)}(r,z)$$
$$u_\theta^{(2)}(r,z) = u_\theta^{(3)}(r,z), \quad \sigma_{r\theta}^{(2)}(r,z) = \sigma_{r\theta}^{(3)}(r,z)$$
$$\sigma_{r\theta}^{(3)}(r,z) = 0$$

Then, Eq. (24) becomes

$$[\mathbf{T}]\{\mathbf{x}\} = \{\mathbf{0}\} \tag{32}$$

where

$$\{\mathbf{x}\} = \{C_1\ D_1\ C_2\ D_2\ C_3\ D_3\ G\}^T$$

$[\mathbf{T}]$ is a 7×7 matrix whose components are calculated using the Appendix A. Solving $\det[\mathbf{T}] = 0$ gives the torsional modes.

3.2. Longitudinal mode vibration

Another simpler mode vibration is called longitudinal mode vibration in which $u_\theta^{(i)} = 0$ and $u_r^{(i)}$ and $u_z^{(i)}$ are independent of θ. This means that the motion is confined to planes perpendicular to the z-axis, which can move, expand and contract in their planes. The solution for the displacement field and stress vector follows from Eqs. (7), (9), (10) and (12)

$$u_r^{(i)} = \frac{\partial \phi_i}{\partial r} - k_z \frac{\partial \chi_i}{\partial r} \tag{33}$$
$$u_z^{(i)} = k_z \phi_i + k_{\psi_i}^2 \chi_i \tag{34}$$
$$\sigma_{rr}^{(i)} = \mu_i \left\{ 2\frac{\partial^2 \phi_i}{\partial r^2} - \frac{\lambda_i \omega^2}{\mu_i c_{L_i}^2} \phi_i - 2k_z \frac{\partial^2 \chi_i}{\partial r^2} \right\} \tag{35}$$
$$\sigma_{rz}^{(i)} = \mu_i \left\{ 2k_z \frac{\partial \phi_i}{\partial r} + \left(k_{\psi_i}^2 - k_z^2\right) \frac{\partial \chi_i}{\partial r} \right\} \tag{36}$$

Thus, the general solution for ϕ_i and χ_i must be constructed from the set

Table 1
Dimensions and mechanical properties of the three-layers model.

	E (Pa)	ρ (kg/m^3)	v	c_f (m/s)	R (m)
Fluid (Blood Ω_f)		1000		1450	0.0105
Intima Ω_1	385.643×10^3	1150	0.45		0.0107
Media Ω_2	1156.928×10^3	1150	0.45		0.0119
Adventitia Ω_3	385.643×10^3	1150	0.45		0.0125

Table 2
The first 16 coupled frequencies f (Hz) of an arterial wall in the case of one-layer model.

No.	(n,m)	Present	FEM	Difference (%)	Mode shape
1	(1,1)	17.37	17.37	0.00	Flexural
2	(2,1)	35.81	35.82	0.02	Breathing
3	(0,1)	40.20	40.20	0.00	Longitudinal
4	(2,2)	45.68	45.69	0.02	Breathing
5	(1,2)	53.10	53.10	0.00	Flexural
6	(2,3)	66.11	66.11	0.00	Breathing
7	(0,2)	77.66	77.66	0.00	Longitudinal
8	(0,1)	79.37	79.37	0.00	Torsional
9	(1,3)	89.27	89.27	0.00	Flexural
10	(2,4)	92.61	92.62	0.01	Breathing
11	(3,1)	104.32	104.35	0.02	Breathing
12	(3,2)	109.56	109.59	0.02	Breathing
13	(0.3)	110.70	110.70	0.00	Longitudinal
14	(3.3)	119.83	119.87	0.03	Breathing
15	(1.4)	120.76	120.76	0.00	Flexural
16	(2.5)	121.52	121.55	0.02	Breathing

$$\phi_i = \left[A_i J_0(k_{\phi_i} r) + B_i Y_0(k_{\phi_i} r)\right] \sin(k_z z) \exp(j\omega t) \tag{37}$$
$$\chi_i = \left[E_i J_0(k_{\psi_i} r) + F_i Y_0(k_{\psi_i} r)\right] \cos(k_z z) \exp(j\omega t) \tag{38}$$

In this case the boundary conditions Eqs. (17)–(23) become

$$\frac{\partial p(r,z)}{\partial r} = \rho_f \omega^2 u_r^{(1)}(r,z)$$
$$\sigma_{rr}^{(1)}(r,z) = -p(r,z), \quad \sigma_{rz}^{(1)}(r,z) = 0$$
$$u_r^{(1)}(r,z) = u_r^{(2)}(r,z), \quad u_z^{(1)}(r,z) = u_z^{(2)}(r,z)$$
$$\sigma_{rr}^{(1)}(r,z) = \sigma_{rr}^{(2)}(r,z), \quad \sigma_{rz}^{(1)}(r,z) = \sigma_{rz}^{(2)}(r,z)$$
$$u_r^{(2)}(r,z) = u_r^{(3)}(r,z), \quad u_z^{(2)}(r,z) = u_z^{(3)}(r,z)$$
$$\sigma_{rr}^{(2)}(r,z) = \sigma_{rr}^{(3)}(r,z), \quad \sigma_{rz}^{(2)}(r,z) = \sigma_{rz}^{(3)}(r,z)$$
$$\sigma_{rr}^{(3)}(r,z) = \sigma_{rz}^{(3)}(r,z) = 0$$

Then, Eq. (24) becomes

$$[\mathbf{L}]\{\mathbf{x}\} = \{\mathbf{0}\} \tag{39}$$

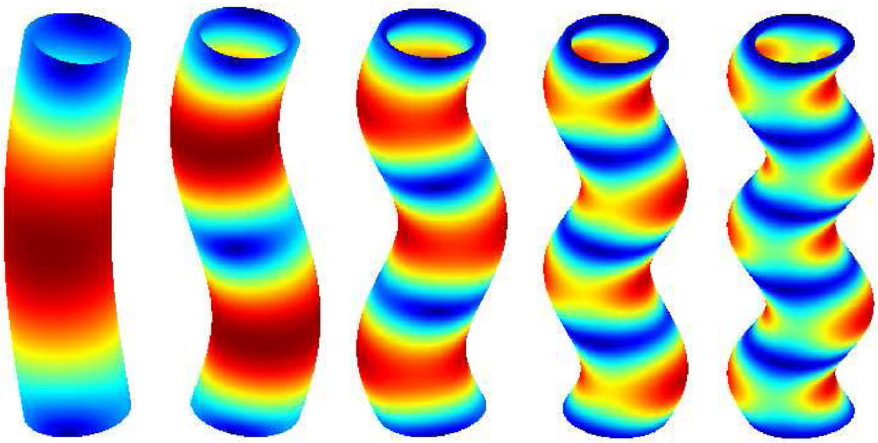

Fig. 3. The flexural coupled modal shapes of arterial wall of (n, m).

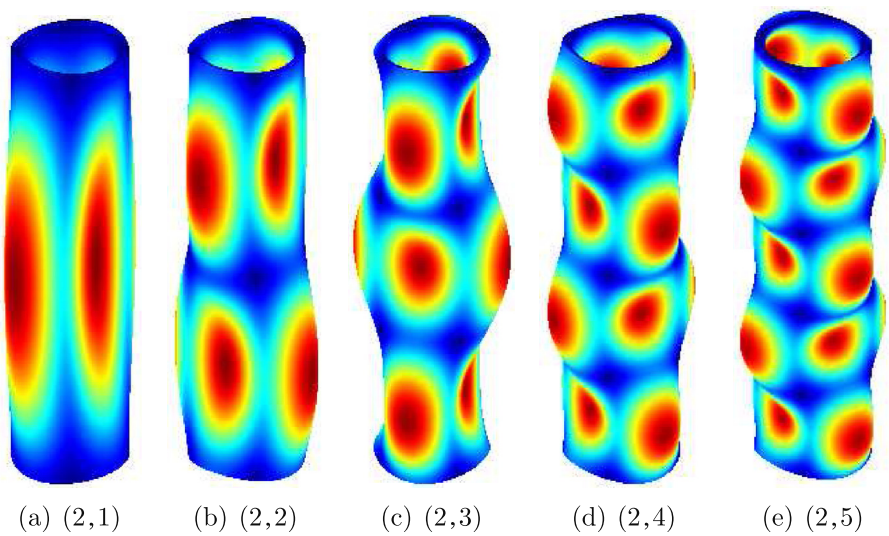

Fig. 4. The breathing coupled modal shapes of arterial wall of (n, m).

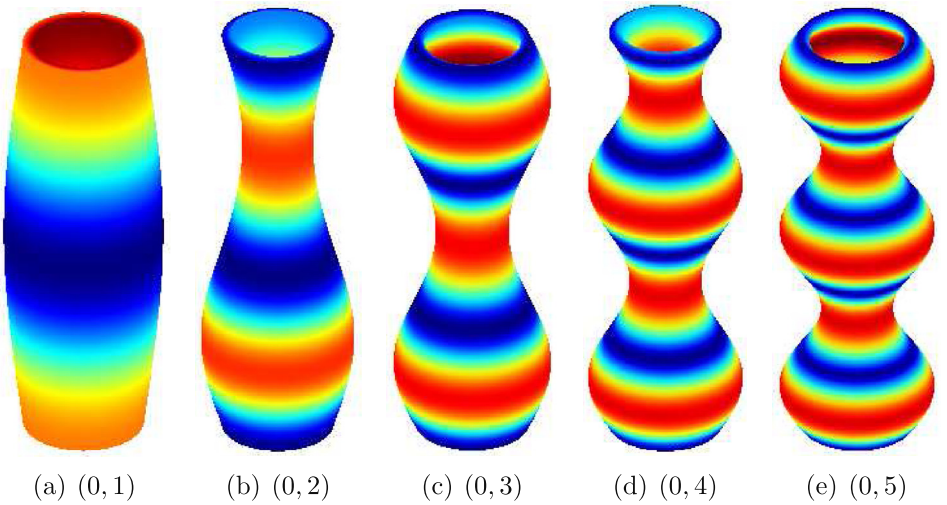

Fig. 5. The longitudinal coupled modal shapes of arterial wall of (n, m).

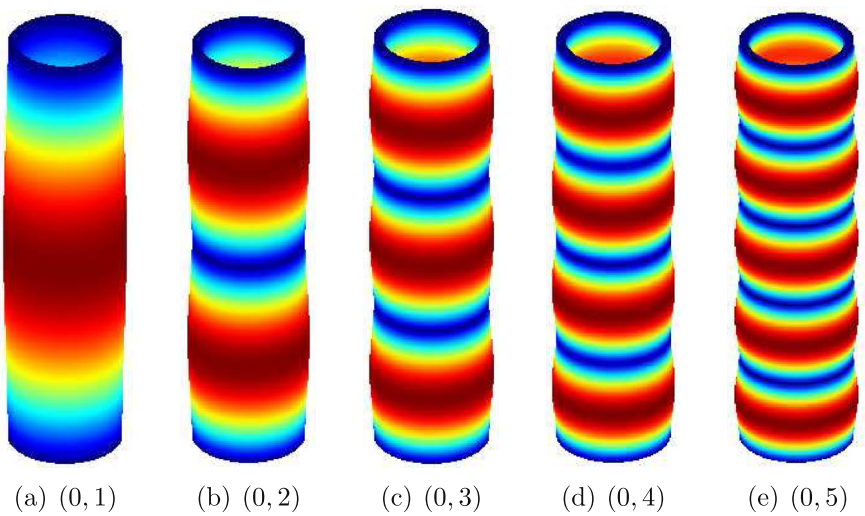

Fig. 6. The torsional modal shapes of arterial wall of (n, m).

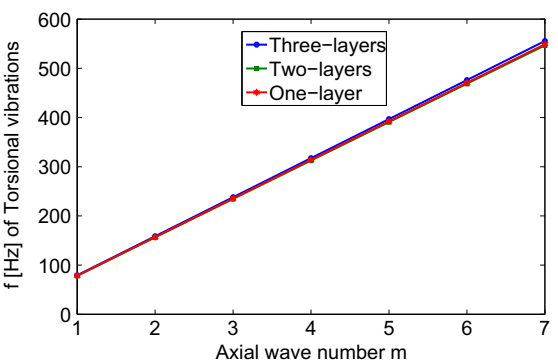

Fig. 7. Variation of the torsional frequencies with m.

where

$$\{\mathbf{x}\} = \{A_1\ B_1\ E_1\ F_1\ A_2\ B_2\ E_2\ F_2\ A_3\ B_3\ E_3\ F_3\ G\}^T$$

$[\mathbf{L}]$ is a 13×13 matrix whose components are calculated using the Appendix A. Solving $\det[\mathbf{L}] = 0$ gives the longitudinal modes.

3.3. Flexural and breathing mode vibrations

The mode shape $n = 1$ is called flexural mode vibration in which all components of the displacement are non-vanishing and depend on $r,\ \theta$ and z. The mode shape $n \geqslant 2$ is called breathing mode vibration in which all components of the displacement are non-vanishing and depend on $r,\ \theta$ and z.

4. Results and discussion

For the numerical examples, geometrical and mechanical properties of the three-layers model are reported on the Table 1 after (Gao et al., 2006). For the two-layers model ($E = 1052.65 \times 10^3$ (Pa)) and one-layer model ($E = 840.366 \times 10^3$ (Pa)) we utilize properties obtained by averaging the different layers stiffness.

With the derived frequency equations, natural frequencies are calculated with the software Mathematica. To validate the analytical results, the coupled natural frequencies and mode shapes are also computed using Comsol Multiphysics Finite Element Analysis Simulation Software. Table 2 shows the comparison of the first sixteen coupled frequencies and the corresponding mode shapes of an arterial wall in the case of one-layer model by FEM (Eq. (24)) and the present method (Eq. (29)). Table 2. In the first sixteen frequencies, four correspond to flexural vibration, eight to breathing vibration, one to torsional vibration and one three longitudinal vibration. The very good agreement is observed between the results of the present method and those of FEM and the maximal relative difference ((FEM-Present)/Present) is only 0.03%.

Figs. 3–6 show, respectively, the first five coupled modal shapes of the flexural, breathing, longitudinal and torsional vibrations. In order to highlight modal shapes, one has increased the scale of visualization. Large deformations on the figures are purely visual. The modal shape can be regarded as the mode (n, m), where n is the modal number in the circumferential

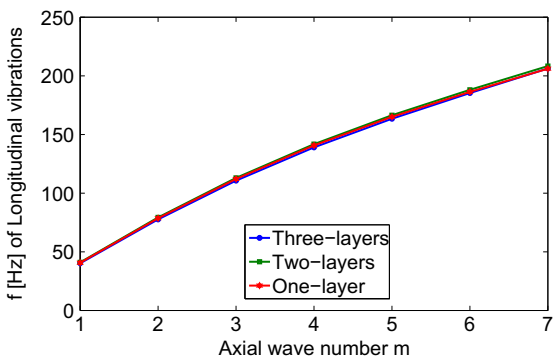

Fig. 8. Variation of the coupled longitudinal frequencies with m.

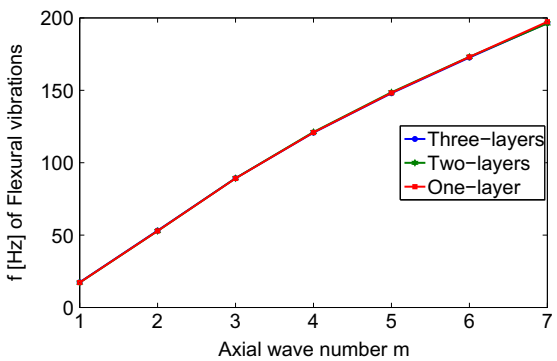

Fig. 9. Variation of the coupled flexural frequencies with m.

direction and m is the modal number in the axial direction. The modal shapes are not in order with the parameters n and m. The frequency of mode (2,2) is lower than that of mode (1,2), for example. This feature of cylindrical vibration is different from that of beam vibration in which the order increases with the modal parameter. Therefore in the vibration of the cylinder, one should be careful as to find the right mode of the vibration.

We observe that modal shapes are not sensibly modified by accounting for multi-layers aspects. But this is probably due to the axisymmetry of the domain. The presence of the fluid has low influence on the modal shapes because the added mass is diagonal. The coupling is light in such a case.

In this paper, the effects of cylindrical parameters on the coupled natural frequencies of cylindrical arterial wall are presented with the present method. In these studies, investigations are carried out to study the effects of circumferential mode n, axial mode m, and multi-layers on the coupled frequencies.

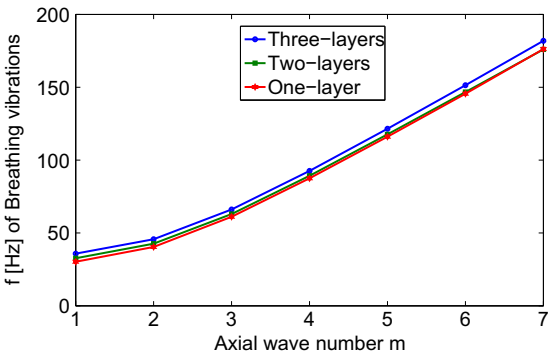

Fig. 10. Variation of the coupled breathing frequencies with m.

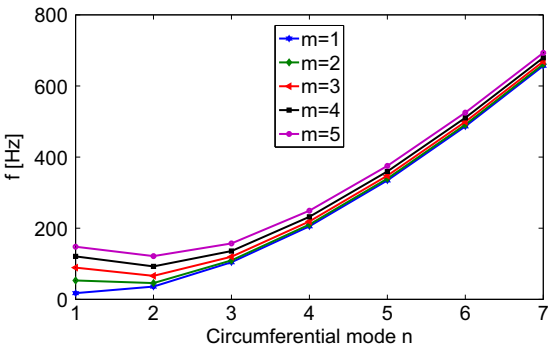

Fig. 11. Variation of the coupled frequency f with n.

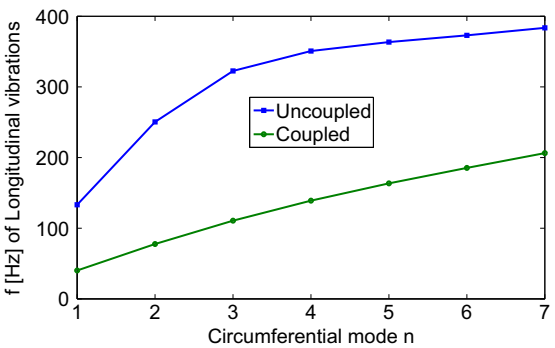

Fig. 12. Variation of the coupled and uncoupled longitudinal frequencies with n.

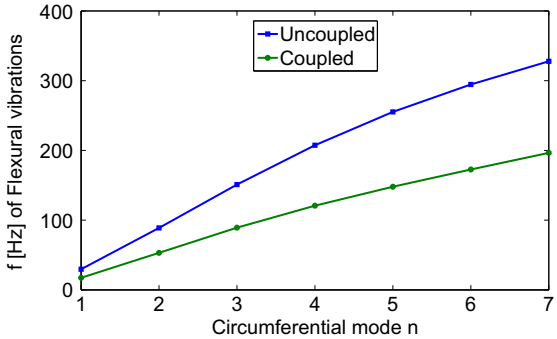

Fig. 13. Variation of the coupled and uncoupled flexural frequencies with n.

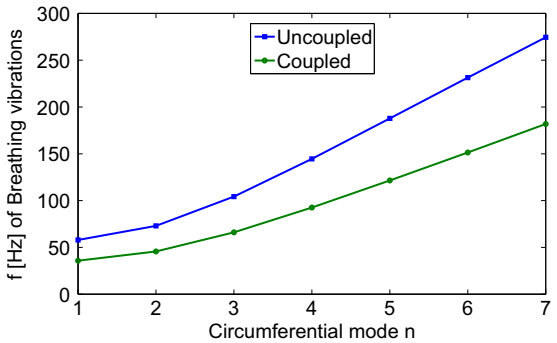

Fig. 14. Variation of the coupled and uncoupled breathing frequencies with n.

Table 3
Variation of the uncoupled breathing frequencies of an arterial wall.

(n, m)	Three-layers	Two-layers	One-layer
$(2, 1)$	49.12	53.15	57.93
$(2, 2)$	64.78	68.38	72.98
$(2, 3)$	96.68	99.91	104.28
$(2, 4)$	136.68	140.09	144.56
$(2, 5)$	178.89	182.99	187.88

First, one investigates how the coupled frequencies for different models vary with the axial mode m. Figs. 7–9 show that, the frequencies increase as the axial mode m increases. The presence of multi-layers do not affect the coupled natural frequencies except the breathing modes vibrations Fig. 10 where we observe a slow variation of the coupled natural frequencies. In the following we study the frequency curves of one-layer model.

Secondly, one investigates how the coupled frequencies vary with the axial mode m and circumferential mode n for one-layer model. Fig. 11 shows that, the coupled frequencies first decrease and then increase as the circumferential mode n increases. All the m frequency curves converge when n is large which means that for large mode n the frequencies are only determined by the n and regardless of the axial mode m.

Thirdly, one investigates how the dense fluid (added mass) affects the frequencies. Figs. 12–14 show the coupled and uncoupled frequencies, varying with the circumferential mode n for one-layer model. As n increases, the difference between the coupled and uncoupled frequencies increases. This behavior is also found for other models.

5. Conclusions

This paper investigates the natural coupled frequency analysis of an aortic injury mechanism. We use analytic and numerical methods for better understanding the mechanisms of this injury. The paper focuses on the biomechanics within the ascending aorta which characterizes the pressure and flow of the entire vascular system (see Fig. 1). Indeed, this branch

is the first part of the system receiving the blood from the heart at the opening of the aortic valve, during the systolic phase. The study and the understanding of the dynamics of this branch are nevertheless complicated due to the fluid–structure coupling effects and due to the radially heterogeneity of the organ (e.g., Pearson et al., 2008). The obtained results have highlighted some points. One-layer model, two-layers model and three-layers model seem to give comparable results with regards of the modal shapes, and the coupled natural frequencies of the coupled aorta-blood are slightly influenced by the presence of multiple layers. The system behavior depends strongly on the boundary conditions. The arterial wall properties (multi-layers) do not modify the natural frequencies. In fact the low variation of frequencies relative to the number of the arterial wall layers is not due to the use of a linear model. But it is mainly due to the two phenomena. On one hand, the stiffness of the fluid provided by the fluid is greater than those of the arterial walls $E_f = \rho_f c_f^2 \simeq 2.10^9$ Pa. On the other hand, the added mass effect plays an important role in the frequency variations (Axisa & Antunes, 2007). Indeed, using the same model of the arterial wall, without fluid, Table 3 shows the sensitivity of the natural frequencies according to the number of arterial layers. Finally this study is designed to analyse the influences of the arterial wall properties (multi-layers) and the blood-aorta interaction rather than to reproduce the complex transient dynamic analysis of the vessels (e.g., Gerbeau, Vidrascu, & Frey, 2005 and Figueroa, Vignon-Clementel, Jansen, Hughes, & Taylor, 2006).

Appendix A

The scalar components of the displacement vector $\mathbf{u}^{(i)}$ in the arterial layers is given in terms of potentials as

$$u_r^{(i)} = \left\{A_i u_1^{(i)}(r) + B_i u_2^{(i)}(r) + E_i u_3^{(i)}(r) + F_i u_4^{(i)}(r) + C_i u_5^{(i)}(r) + D_i u_6^{(i)}(r)\right\} \cos(n\theta) \sin(k_z z) \exp(j\omega t) \tag{A.1}$$

$$u_\theta^{(i)} = \left\{A_i v_1^{(i)}(r) + B_i v_2^{(i)}(r) + E_i v_3^{(i)}(r) + F_i v_4^{(i)}(r) + C_i v_5^{(i)}(r) + D_i v_6^{(i)}(r)\right\} \sin(n\theta) \sin(k_z z) \exp(j\omega t) \tag{A.2}$$

$$u_z^{(i)} = \left\{A_i w_1^{(i)}(r) + B_i w_2^{(i)}(r) + E_i w_3^{(i)}(r) + F_i w_4^{(i)}(r)\right\} \times \cos(n\theta) \cos(k_z z) \exp(j\omega t) \tag{A.3}$$

The stress tensor in the arterial layers $\sigma(\mathbf{u}^{(i)})$ is given by Hooke's law in terms of potentials as

$$\sigma_{rr}^{(i)} = \left\{A_i S_1^{(i)}(r) + B_i S_2^{(i)}(r) + E_i S_3^{(i)}(r) + F_i S_4^{(i)}(r) + C_i S_5^{(i)}(r) + D_i S_6^{(i)}(r)\right\} \cos(n\theta) \sin(k_z z) \exp(j\omega t) \tag{A.4}$$

$$\sigma_{r\theta}^{(i)} = \left\{A_i T_1^{(i)}(r) + B_i T_2^{(i)}(r) + E_i T_3^{(i)}(r) + F_i T_4^{(i)}(r) + C_i T_5^{(i)}(r) + D_i T_6^{(i)}(r)\right\} \sin(n\theta) \sin(k_z z) \exp(j\omega t) \tag{A.5}$$

$$\sigma_{rz}^{(i)} = \left\{A_i Z_1^{(i)}(r) + B_i Z_2^{(i)}(r) + E_i Z_3^{(i)}(r) + F_i Z_4^{(i)}(r) + C_i Z_5^{(i)}(r) + D_i Z_6^{(i)}(r)\right\} \cos(n\theta) \cos(k_z z) \exp(j\omega t) \tag{A.6}$$

where

$$u_1^{(i)}(r) = J_n'(k_{\phi_i} r), \quad u_3^{(i)}(r) = -k_z J_n'(k_{\psi_i} r), \quad u_5^{(i)}(r) = \frac{n}{r} J_n(k_{\psi_i} r) \tag{A.7}$$

$$u_2^{(i)}(r) = Y_n'(k_{\phi_i} r), \quad u_4^{(i)}(r) = -k_z Y_n'(k_{\psi_i} r), \quad u_6^{(i)}(r) = \frac{n}{r} Y_n(k_{\psi_i} r) \tag{A.8}$$

$$v_1^{(i)}(r) = -\frac{n}{r} J_n(k_{\phi_i} r), \quad v_3^{(i)}(r) = \frac{n k_z}{r} J_n(k_{\psi_i} r), \quad v_5^{(i)}(r) = -J_n'(k_{\psi_i} r) \tag{A.9}$$

$$v_2^{(i)}(r) = -\frac{n}{r} Y_n(k_{\phi_i} r), \quad v_4^{(i)}(r) = \frac{n k_z}{r} Y_n(k_{\psi_i} r), \quad v_6^{(i)}(r) = -Y_n'(k_{\psi_i} r) \tag{A.10}$$

$$w_1^{(i)}(r) = k_z J_n(k_{\phi_i} r), \quad w_3^{(i)}(r) = k_{\psi}^2 J_n(k_{\psi_i} r) \tag{A.11}$$

$$w_2^{(i)}(r) = k_z Y_n(k_{\phi_i} r), \quad w_4^{(i)}(r) = k_{\psi_i}^2 Y_n(k_{\psi_i} r) \tag{A.12}$$

$$S_1^{(i)}(r) = 2\mu_i \left[J_n''(k_{\phi_i} r) - \frac{\lambda_i \omega^2}{2\mu_i c_{L_i}^2} J_n(k_{\phi_i} r)\right] \tag{A.13}$$

$$S_2^{(i)}(r) = 2\mu_i \left[Y_n''(k_{\phi_i} r) - \frac{\lambda_i \omega^2}{2\mu_i c_{L_i}^2} Y_n(k_{\phi_i} r)\right] \tag{A.14}$$

$$S_3^{(i)}(r) = -2k_z \mu_i J_n''(k_{\psi_i} r), \quad S_5^{(i)}(r) = \frac{2n\mu_i}{r^2} \left[r J_n'(k_{\psi_i} r) - J_n(k_{\psi_i} r)\right] \tag{A.15}$$

$$S_4^{(i)}(r) = -2k_z \mu_i Y_n''(k_{\psi_i} r), \quad S_6^{(i)}(r) = \frac{2n\mu_i}{r^2} \left[r Y_n'(k_{\psi_i} r) - Y_n(k_{\psi_i} r)\right] \tag{A.16}$$

$$T_1^{(i)}(r) = \frac{2n\mu_i}{r^2}\left[J_n(k_{\phi_i}r) - rJ'_n(k_{\phi_i}r)\right] \tag{A.17}$$

$$T_2^{(i)}(r) = \frac{2n\mu_i}{r^2}\left[Y_n(k_{\phi_i}r) - rY'_n(k_{\phi_i}r)\right] \tag{A.18}$$

$$T_3^{(i)}(r) = \frac{2nk_z\mu_i}{r^2}\left[rJ'_n(k_{\psi_i}r) - J_n(k_{\psi_i}r)\right] \tag{A.19}$$

$$T_4^{(i)}(r) = \frac{2nk_z\mu_i}{r^2}\left[rY'_n(k_{\psi_i}r) - Y_n(k_{\psi_i}r)\right] \tag{A.20}$$

$$T_5^{(i)}(r) = -\mu_i\left[2J''_n(k_{\psi_i}r) + k_{\psi_i}^2 J_n(k_{\psi_i}r)\right] \tag{A.21}$$

$$T_6^{(i)}(r) = -\mu_i\left[2Y''_n(k_{\psi_i}r) + k_{\psi_i}^2 Y_n(k_{\psi_i}r)\right] \tag{A.22}$$

$$Z_1^{(i)}(r) = 2\mu_i k_z J'_n(k_{\phi_i}r), \quad Z_3^{(i)}(r) = \mu_i\left(k_{\psi_i}^2 - k_z^2\right)J'_n(k_{\psi_i}r) \tag{A.23}$$

$$Z_2^{(i)}(r) = 2\mu_i k_z Y'_n(k_{\phi_i}r), \quad Z_4^{(i)}(r) = \mu_i\left(k_{\psi_i}^2 - k_z^2\right)Y'_n(k_{\psi_i}r) \tag{A.24}$$

$$Z_5^{(i)}(r) = \frac{nk_z\mu_i}{r}J_n(k_{\psi_i}r), \quad Z_6^{(i)}(r) = \frac{nk_z\mu_i}{r}Y_n(k_{\psi_i}r) \tag{A.25}$$

References

Axisa, F., & Antunes, J. (2007). *Modeling of mechanical systems: Fluid structure interaction* (Vol. 3). Elsevier.

Bathe, K. J. (1996). *Finite element procedures*. Prentice Hall.

Figueroa, C. A., Vignon-Clementel, I. E., Jansen, K. E., Hughes, T. J. R., & Taylor, C. A. (2006). A coupled momentum method for modelling blood flow in three-dimensional deformables arteries. *Computer Methods in Applied Mechanics and Engineering, 195*, 5685–5706.

Forman, J., Stacey, S., Evans, J., & Kent, R. (2008). Posterior acceleration as a mechanism of blunt traumatic injury of the aorta. *Journal of Biomechanics, 41*, 1359–1364.

Gao, F., Guo, Z., Sakamoto, M., & Matsuzawa, T. (2006). Fluid-structure interaction within a layered aortic arch model. *Journal of Biological Physics, 32*, 435–454.

Gerbeau, J. F., Vidrascu, M., & Frey, P. (2005). Fluid-structure interaction in blood flows on geometries based on medical imaging. *Journal of Biological Physics, 83*, 155–165.

Hamdi, M. A., Ousset, Y., & Verchery, G. (1978). A displacement method for analysis of vibrations of coupled fluid-structure systems. *International Journal for Numerical Methods in Engineering, 13*, 139–150.

Holzapfel, G. A. (2006). *Structural and numerical models for the (visco)elastic response of arterial walls with residual stresses. Biomechanics of soft tissue in cardiovascular system*. New York: Springer (pp. 109–184).

Holzapfel, G. A., & Gasser, T. C. (2007). Computational stress-deformation analysis of arterial walls including high-pressure response. *International Journal of Cardiology, 116*(1), 78–85.

Mellado, M., & Rodrguez, R. (2001). Efficient solution of fluid–structure vibration problems. *Applied Numerical Mathematics, 36*, 389–400.

Moore, J. E., Guggenheim, N., Delfino, A., Doriot, P. A., Dorsaz, P. A., Rutishauser, W., et al (2008). Preliminary analysis of the effects of blood vessel movement on blood flow patterns in the coronary arteries. *Journal of Biomechanical Engineering, 116*, 302–306.

Morand, H. J.-P., & Ohayon, R. (1979). Substructure variational analysis of the vibrations of coupled fluid-structure systems: finite element results. *International Journal for Numerical Methods in Engineering, 14*, 741–755.

Morand, H. J.-P., & Ohayon, R. (1995). *Fluid structure interaction*. John Wiley & Sons.

Morse, M., & Feshbach, H. (1946). *Methods of theoretical physics*. New York: McGraw-Hill.

Ou, P., Balleux, F., Jolivet, O., Herment, A., Sidi, D., Bonnet, D., et al (2005). Substructure variational analysis of the vibrations of coupled fluid-structure systems: finite element results. *International Journal for Numerical Methods in Engineering, 98*(7–8), 957–968.

Parthasarathi, A. A., Grosh, K., & Nuttall, A. L. (2000). Three-dimensional numerical modeling for global cochlear dynamics. *Journal of the Acoustical Society of America, 107*, 474–485.

Pearson, R., Philips, N., Hancock, R., Hashim, S., Field, M., Richens, D., et al (2008). Regional wall mechanics and blunt traumatic aortic rupture in the isthmus. *European Journal of Cardio-Thoracic Surgery, 34*, 616–622.

Prosi, M., Perktold, K., Ding, Z., & Friedman, M. H. (2004). Influence of curvature dynamics on pulsatile coronary artery flow in a realistic bifurcation model. *Journal of Biomechanics, 37*, 1767–1775.

Tsai, C. C., Young, D. L., Chen, C. W., & Fan, C. M. (2006). The method of fundamental solutions for eigenproblems in domains with and without holes. *Proceedings of the Royal Society of London, 462*, 1443–1466.

Zhang, X. M. (2002). Parametric studies of coupled vibration of cylindrical pipes conveying fluid with the wave propagation approach. *Computers and Structures, 80*, 287–295.

Zhang, X. M., Liu, G. R., & Lam, K. Y. (2001). An anisotropic model for frequency analysis of arterial walls with the wave propagation approach. *Journal of Sound and Vibration, 239*(3), 397–403.

Zhao, A. R., Field, M. L., Diggers, K., & Richens, D. (2008). Blunt trauma and acute aortic syndrome: A three-layer finite-element model of the aortic wall. *European Journal of Cardio-Thoracic Surgery, 34*, 623–629.

Zienkiewich, O. C., & Taylor, R. L. (1989). *The finite element method* (Vol. 2). McGraw-Hill.